Local Atmospheric Response to an Open-Ocean Polynya in a High-Resolution Climate Model

Wilbert Weijer and Milena Veneziani

Los Alamos National Laboratory, Los Alamos, New Mexico

Achim Stössel

Texas A&M University, College Station, Texas

Matthew W. Hecht, Nicole Jeffery, and Alexandra Jonko

Los Alamos National Laboratory, Los Alamos, New Mexico

Travis Hodos

U.S. Air Force Academy, Colorado Springs, Colorado

Hailong Wang

Pacific Northwest National Laboratory, Richland, Washington

(Manuscript received 6 February 2016, in final form 28 October 2016)

ABSTRACT

In this paper the atmospheric response to an open-ocean polynya in the Southern Ocean is studied by analyzing the results from an atmospheric and oceanic synoptic-scale resolving Community Earth System Model (CESM) simulation. While coarser-resolution versions of CESM generally do not produce open-ocean polynyas in the Southern Ocean, they do emerge and disappear on interannual time scales in the synoptic-scale simulation. This provides an ideal opportunity to study the polynya's impact on the overlying and surrounding atmosphere. This has been pursued here by investigating the seasonal cycle of differences of surface and air-column variables between polynya and nonpolynya years. The results indicate significant local impacts on turbulent heat fluxes, precipitation, cloud characteristics, and radiative fluxes. In particular, it is found that clouds over polynyas are optically thicker and higher than clouds over sea ice during nonpolynya years. Although the lower albedo of polynyas significantly increases the net shortwave absorption, the enhanced cloud brightness tempers this increase by almost 50%. Also, in this model, enhanced longwave radiation emitted from the warmer surface of polynyas is balanced by stronger downwelling fluxes from the thicker cloud deck. Impacts are found to be sensitive to the synoptic wind direction. The strongest regional impacts are found when northeasterly winds cross the polynya and interact with katabatic winds. Surface air pressure anomalies over the polynya are only found to be significant when cold, dry air masses strike over the polynya (i.e., in the case of southerly winds).

1. Introduction

Polynyas are areas of open water enclosed by the seasonal ice pack (and oftentimes the coast). They facilitate a strong heat exchange between the atmosphere and ocean, and often feature intense sea ice production. Antarctic polynyas are thought to play a key role in the formation of Antarctic Bottom Water (AABW; Zwally et al. 1985), the most voluminous water mass in the World Ocean (Johnson 2008). Polynyas also often sustain high levels of biological productivity (e.g., Smith and Gordon 1997; Arrigo and Van Dijken 2003).

Coastal polynyas are a ubiquitous feature of the Antarctic coastal environment, as in many places cold katabatic winds push newly formed sea ice away from the land, keeping the coastal waters virtually ice free

---

ⓐ Denotes content that is immediately available upon publication as open access.

Corresponding author e-mail: Wilbert Weijer, wilbert@lanl.gov

(e.g., Adolphs and Wendler 1995). Open-ocean polynyas are more enigmatic, as they require an ocean heat source to keep the polynya ice free. The most spectacular example is the Weddell Polynya, a large persistent polynya that was observed in the mid-1970s, but has not appeared since (Zwally and Gloersen 1977; Carsey 1980). This polynya was associated with deep convection that tapped into the heat of the relatively warm Weddell Sea Deep Water, which is modified Circumpolar Deep Water supplied by the Weddell Gyre (Martinson et al. 1981; Gordon 1982); it may have been preconditioned by anomalous atmospheric conditions associated with a prolonged negative phase of the southern annular mode (Gordon et al. 2007), and triggered by ocean–topography interaction at Maud Rise (Holland 2001). de Lavergne et al. (2014) argue that the Weddell Polynya may have previously occurred before its mid-1970s observation and subsequent disappearance, in particular around 1960, implying that deep convection may have been a natural mode of ventilation before the mid-1970s. If so, the absence of the Weddell Polynya since that time would have to be understood as representing a significant regime shift that would be convolved with other changes involving deep waters today (e.g., Gordon 2014).

Smaller open-ocean polynyas like the Maud Rise and Cosmonaut Polynya are in general more transient (e.g., Comiso and Gordon 1987). Comiso and Gordon (1996) argue that the Cosmonaut Polynya results from the upwelling of warm water induced by vortex stretching, which is required to balance the enhanced shear that develops when Cape Ann forces the westward Antarctic Coastal Current northward onto the eastward Antarctic Circumpolar Current. More recent studies suggest that the polynya may have been forced by synoptic atmospheric variability instead, with transient low pressure systems causing both a divergence of sea ice transport (Arbetter et al. 2004; Bailey et al. 2004), and Ekman-induced upwelling of warm waters (Prasad et al. 2005). The Maud Rise Polynya has been interpreted as the result of an interaction between the background flow and the Maud Rise, a seamount that rises to a depth of 2000 m (e.g., Gordon and Haxby 1990). In particular, Holland (2000, 2001) argues that cyclonic eddies spawned from this interaction lead to divergent sea ice transport, and may have triggered the intense air–sea interaction that led to the persistent Weddell Sea Polynya of the mid-1970s. Reviews of polynya studies can be found in Smith et al. (1990), Maqueda et al. (2004), and Williams et al. (2007).

It is important to understand the conditions under which polynyas form, and the effect that they have on the state of the ocean and atmosphere. In fact, the current generation of climate models varies widely in its representation of polynyas and the convective state of the Weddell Sea in particular (Heuzé et al. 2013; de Lavergne et al. 2014; Downes et al. 2015; Stössel et al. 2015). Even different configurations of the same model code (e.g., with eddying and noneddying resolutions) can exhibit contrasting behavior, as is the case with the model used for this study. The impact of open-ocean polynyas on the stratification of the Southern Ocean and the characteristics of Antarctic Bottom Water has been the subject of several studies (e.g., Stössel et al. 2002; Heuzé et al. 2013; Downes et al. 2015). Yet, it remains an open question to what extent the presence or absence of polynyas can account for differences in the mean state of the atmosphere.

The atmospheric response to polynyas has been the subject of several process studies. Dare and Atkinson (1999, 2000) show how turbulent heat fluxes increase the buoyancy over the polynya, generating a turbulent plume that mixes high-momentum air downward. The resulting acceleration of the flow over the polynya leads to divergence and downdrafts on the upwind side of the polynya, and convergence and updrafts on the downwind side. The increased flow speed is aided by reduced surface drag over the open water compared to the surrounding ice pack (Andreas et al. 1984).

Working within the limitations of sparse observational data, Moore et al. (2002) reconstruct the atmospheric response to the 1976 Weddell Polynya using a reanalysis of the atmospheric state during the period of its presence. They report 20°C warmer air temperatures and 20% more cloud cover over the Weddell Polynya compared to climatology and sensible and latent heat flux anomalies on the order of 150 and 50 W m^{-2}, respectively. Timmermann et al. (1999) argue that the thermal anomaly caused by such excessive turbulent heat fluxes can generate a low pressure anomaly over the polynya. Indeed, Moore et al. (2002) find a 6–8-hPa reduction in sea level pressure over the Weddell Polynya compared to climatology. Glowienka-Hense (1995) shows that this thermal anomaly can even have global impacts. She uses a coarse-resolution atmospheric general circulation model and finds that a sea surface temperature (SST) anomaly representative of the Weddell Polynya can lead to significant changes in the global circulation; in particular a deepening of the circumpolar trough between 40° and 60°S, and an overall intensification of the mean circulation globally.

There is a continuing push of coupled climate models toward higher resolutions (e.g., McClean et al. 2011; Delworth et al. 2012), and a few groups now have run fully coupled eddy-resolving simulations for a century or

longer (e.g., Kirtman et al. 2012; Griffies et al. 2015). Here we will take advantage of such a state-of-the-art high-resolution climate simulation (Small et al. 2014) to refine estimates of the impact of a large open-ocean polynya in the Southern Ocean on the atmosphere. It must be kept in mind that climate models, despite much progress in recent years (e.g., Kay et al. 2012), still have significant biases, in particular in the radiative balance of the Southern Ocean. This can be largely ascribed to well-known difficulties in the representation of mixed-phase clouds, where ice and supercooled liquid coexist (Komurcu et al. 2014; Kay et al. 2016; Tan et al. 2016). But even though it is understood that the model is an imperfect representation of nature, we believe that detailed analysis of a high-resolution model can provide useful qualitative and quantitative insights into the impact of polynyas on the atmosphere.

The aim of this paper is to (i) investigate and quantify the local atmospheric response to polynyas in a comprehensive, synoptic-scale resolving climate model; and by doing so (ii) document some aspects of the atmosphere over the high-latitude Southern Ocean in this model. In section 2 we will briefly introduce the model, the simulation, and our analysis approach. Results are presented in section 3. First we study the seasonal evolution of atmospheric conditions over polynyas, and compare them to conditions over sea ice during nonpolynya years. This analysis is followed by a detailed look at the differences in the vertical structure of the atmosphere during the August–September–October (ASO) trimester. Finally, using daily-averaged data, we study how the atmospheric response depends on the synoptic wind direction over the polynya. In section 4 we summarize and discuss our findings.

2. Methods

To study the atmospheric response to a large polynya in the Southern Ocean, we use output from the high-resolution coupled climate system simulation described by Small et al. (2014). The Community Earth System Model, version 1 (CESM1), they employed is widely used for investigations of climate variability and change (e.g., Hurrell et al. 2013; Kay et al. 2015). This simulation was run during the Accelerated Scientific Discovery (ASD) phase of the platform Yellowstone, and is among the first efforts to run CESM1 in a high-resolution configuration that explicitly resolves mesoscale features in the ocean. The ocean component is the Parallel Ocean Program, version 2 (POP2), configured at a nominal resolution of 0.1°. It is coupled to a sea ice simulator at the same resolution, the Los Alamos Sea Ice Model version 4 (CICE4). The atmosphere component is the

Community Atmosphere Model, version 5 (CAM5), configured at an approximate 0.25° resolution of the Spectral Element (SE) dynamical core. The model was run for 100 years under fixed radiative forcing conditions representative of the year 1990. Most model fields were saved as monthly averages, but a limited number of variables are available as daily averages. A companion run at nominal (and standard) 1° ocean and atmosphere resolutions did not produce open-ocean polynyas in any year, and is hence not considered in this study.

In the first decades of the high-resolution simulation, the ice pack in the Southern Ocean is quite unrealistic, with large areas of open water in the Weddell Sea in winter. In subsequent years the sea ice cover becomes more realistic, although it remains highly variable. Polynyas fully enclosed by sea ice or embayments connected to the greater (ice free) Southern Ocean are featured in most years; years with a full ice cover are rare.

A polynya is defined here as an enclosed region within the Antarctic ice pack that has ice fractions below 15%. For this study we selected three simulation years (68, 76, and 80) that feature a polynya that is fully enclosed by the solid ice pack for at least the 3-month period of ASO (i.e., the months that feature the highest overall sea ice concentrations) (Fig. 1). The polynyas in these 3 years appear approximately at the same location (between 64°–68°S latitude and 0°–20°E longitude) and are comparable in size (1.1, 0.8, and 1.4×10^5 km², respectively) to the Maud Rise Polynya that appeared in 1980 (0.9×10^5 km² Comiso and Gordon 1987). They are a factor of 2–3 smaller than the polynyas observed in the Weddell Sea between 1974 and 1976 ($2-3 \times 10^5$ km²; Carsey 1980). For calculating polynya-averaged quantities, we define polynya masks based on the 15% contour of the ASO-averaged sea ice fraction for each year.

To distinguish the impact of the polynyas on the overlying and surrounding atmosphere, we contrast the associated atmospheric conditions with those emerging in nonpolynya years. To that end, we also selected three years with full sea ice cover (63, 64, and 72). To compare polynya-averaged atmospheric quantities with representative nonpolynya conditions we define a mask for those nonpolynya years that roughly represents the size and location of the polynyas during the three polynya years. We constructed this "polynya mask" for nonpolynya years by averaging the ASO sea ice fractions of the three polynya years, and taking the 45% contour to make sure that the mask encompasses the region covered by the three individual polynyas (red contours in Fig. 1).

We show the annual time series of polynya-averaged atmospheric quantities, as well as vertical profiles of polynya-averaged quantities for the ASO trimester. Given the low number of degrees of freedom associated with
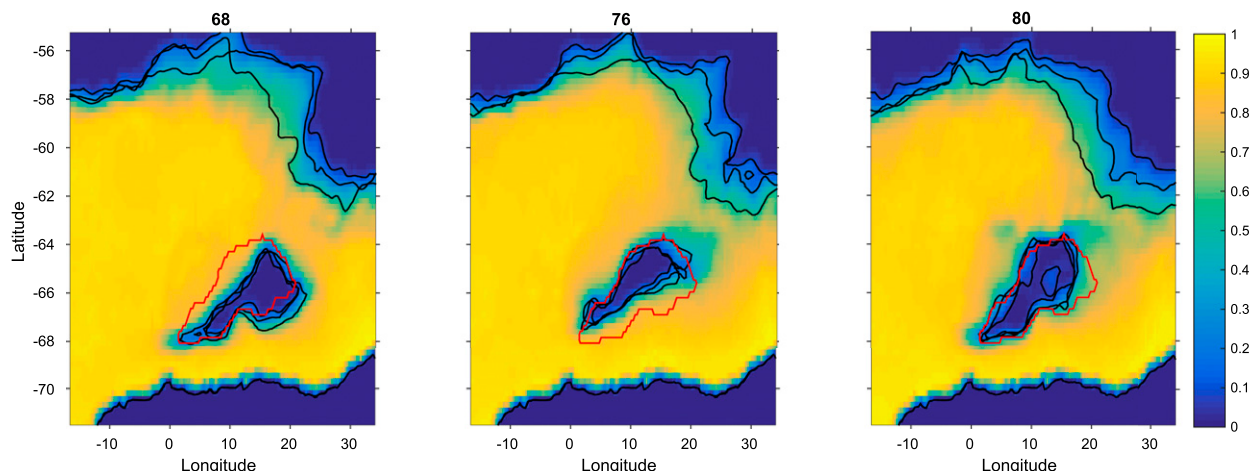
FIG. 1. Shading shows sea ice fraction for the three polynya years, averaged over the ASO trimester. Black contours indicate the 15% limits of sea ice concentration for these individual months, and show that the polynyas are stable in size, shape, and location during this entire 3-month period. The red contours indicate the canonical "polynya mask" used for nonpolynya years, and is representative of the size, shape, and location of the three polynyas; it is based on the 45% contour of sea ice fraction averaged over all three polynya years. The "island" in year 80 reflects an area of elevated (30%) sea ice fraction within the polynya during August of that year.

just a few years' worth of monthly averaged quantities, no attempt was made to formally test the significance of the difference between the means. If the means of the two sets (polynya/nonpolynya years) are outside the envelopes of each other's individual years, we call them "significantly different," although this may not necessarily be true in a strictly statistical sense.

We also perform an additional analysis to understand the sensitivity of the atmospheric response to the synoptic wind direction. This directional analysis is based on the daily direction of the winds over the polynya, which is calculated from the polynya-averaged components of the surface velocity. We divide the daily averaged fields into five directional categories. The category referred to as central (CE) consists of days for which the polynya-averaged winds are less than $5\,\mathrm{m\,s^{-1}}$, regardless of direction. The northeasterly (NE), northwesterly (NW), southwesterly (SW), and southeasterly (SE) categories refer to days during which polynya-averaged winds exceed $5\,\mathrm{m\,s^{-1}}$ and come from the indicated direction. Differences between means are tested using the Student's t test, following von Storch and Zwiers (1999, p. 112).

3. Results

a. Seasonal evolution: Polynya versus nonpolynya years

Figure 2 shows the annual evolution of several atmospheric variables, for polynya (red) and nonpolynya (blue) years. For nonpolynya years, ice fraction passes through the 15% level in June, and reaches 90% in September; by design, polynya-averaged sea ice fractions remain below 15% for polynya years. The polynyas are very stable in their extent and shape, and remain consistently ice free throughout the winter and spring seasons. This suggests that the cause of the polynya is oceanic in nature, and that synoptic atmospheric variability is not responsible for maintaining the polynya. This is in contrast to the role often ascribed to synoptic atmospheric variability in the generation and maintenance of the highly variable Cosmonaut Polynya (Arbetter et al. 2004; Bailey et al. 2004; Prasad et al. 2005). However, it does not preclude the possibility that interannual and large-scale variability of the atmosphere (as represented, for instance by the southern annular mode) plays a role in the generation and maintenance of the polynya through its impact on the Weddell Gyre (e.g., Gordon et al. 2007; Cheon et al. 2014, 2015).

Surface temperatures (TS) differ strongly between polynya and nonpolynya years; TS in polynya years is limited by the freezing temperature of seawater ($\approx 271\,\mathrm{K}$), while the surface of the sea ice in nonpolynya years dips down to $257\,\mathrm{K}$. Near-surface air temperatures (TBOT) drop to only $265\,\mathrm{K}$ for polynya years whereas they get as low as $257\,\mathrm{K}$ for nonpolynya years; TS and TBOT are hence almost equalized for nonpolynya years, while a significant $[\mathcal{O}(6K)]$ temperature contrast persists over polynyas. The higher atmospheric surface temperatures are also reflected in the specific humidity (QBOT), which is significantly higher for the August–November period during polynya years.

The absence of sea ice cover in polynya years has a clear impact on the balance of sensible (SHFLX) and latent (LHFLX) heat fluxes (defined here as positive if
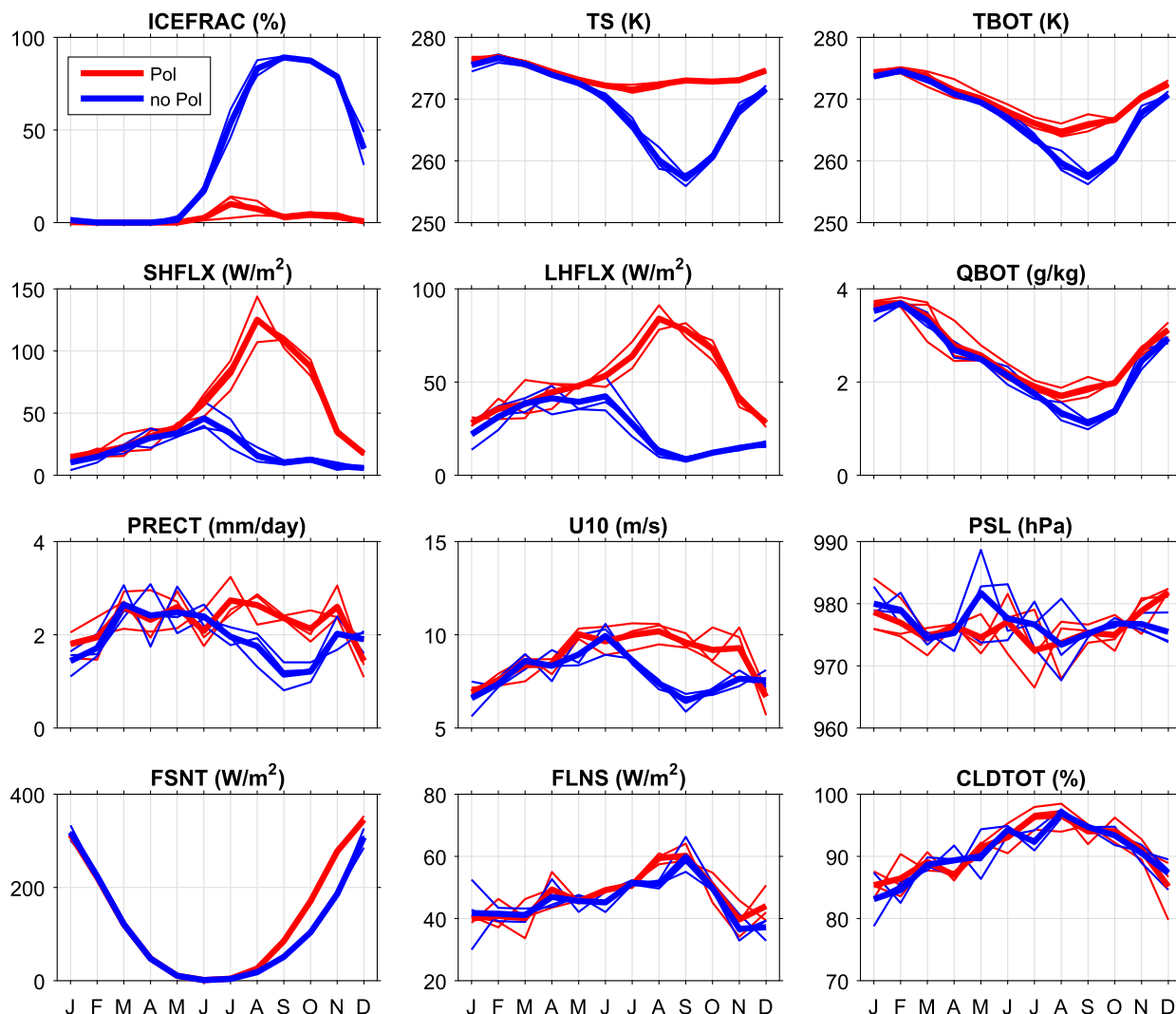
FIG. 2. Seasonal evolution of sea ice fraction (ICEFRAC) and different atmospheric variables for the three polynya years (thin red), the three nonpolynya years (thin blue), and their averages (thick lines). Shown are monthly averaged values. Variables shown are surface temperature (TS), atmospheric temperature at the near-surface (TBOT), sensible (SHFLX) and latent (LHFLX) heat flux, specific humidity at the near-surface (QBOT), precipitation rate (PRECT), wind speed at 10 m (U10), atmospheric surface pressure (PSL), net shortwave balance at the top of the atmosphere (FSNT), net longwave balance at the surface (FLNS), and total cloud fraction (CLDTOT).

toward the atmosphere). After a gradual increase in the first 5 months, these turbulent fluxes sharply decrease after mid-June during nonpolynya years. This is mostly due to the increase in sea ice thickness that prevents effective heat exchange between the ocean and atmosphere. SHFLX hovers around $10 \, \mathrm{W \, m^{-2}}$ from August onward, while LHFLX bottoms out below $10 \, \mathrm{W \, m^{-2}}$ in early September. For polynya years, SHFLX peaks in August at $125 \, \mathrm{W \, m^{-2}}$ and LHFLX peaks at $85 \, \mathrm{W \, m^{-2}}$. So sensible and latent heat fluxes are typically 110 and $72 \, \mathrm{W \, m^{-2}}$ higher in polynya years compared to nonpolynya years. Integrated over the polynya area and over the year, the excess sensible and latent heat transfer is 114 EJ ($1 \, \mathrm{EJ} = 10^{18} \, \mathrm{J}$) and 87 EJ, respectively.

Polynyas experience more precipitation (PRECT; roughly by $1 \, \mathrm{mm \, day^{-1}}$) from July to November, and maintain strong 10-m wind speeds (U10), but they do not seem to have an impact on the local surface pressure distribution (PSL), or on the pressure field aloft (not shown). The rapid decline in U10 during nonpolynya years between June and September coincides with the increase in sea ice concentration, and may be a result of enhanced surface friction over sea ice compared to the ice-free ocean (Andreas et al. 1984). There may also be a dynamical reason for reduced surface winds over sea ice, as explained by Dare and Atkinson (1999): weaker turbulent heat fluxes stabilize the atmospheric boundary layer, preventing stronger winds from aloft from being

mixed downward, reducing surface wind speeds. This dynamical impact is consistent with the fact that the southerly wind directions in our directional analysis below display the largest turbulent flux anomalies over polynyas and the most significant enhancements in U10. It is possible that interannual changes in the large-scale atmospheric circulation may to some extent control the absence or presence of polynyas in this model, and that those changes are imprinted on the time series. The directional analysis below (Fig. 6) indeed appears to show enhanced wind speeds over a broad region for all wind directions, but there are clear local enhancements over the polynyas, suggesting that at least part of the signal in U10 is a response to polynyas.

Polynyas have a pronounced impact on the net shortwave radiation budget at the top of the atmosphere (FSNT). Indeed, the ocean surface within polynyas strongly reduces the albedo and increases absorption of shortwave solar radiation. The difference of the net shortwave balance between polynya and nonpolynya years has a seasonally asymmetric evolution (Fig. 3). It peaks in November when the incoming solar radiation is sufficiently strong and the retreating ice pack still sufficiently expansive for an optimal response. Peak values are 91 W m^{-2} at the top of the atmosphere, and just 3 W m^{-2} higher at the surface (FSNS). The net shortwave energy uptake by the ocean is 67 EJ more during polynya years.

To investigate to what extent this difference is caused by changes in surface albedo, or whether clouds play a role as well, we consider the clear-sky fluxes, which are routinely diagnosed in the CAM5 atmosphere model by repeating the radiative transfer calculations without clouds. The net shortwave budgets at the surface (FSNSC) and top of the atmosphere (FSNTC) under clear-sky conditions is significantly higher than under full-sky conditions, and peak at 164 and 158 W m^{-2}, respectively. Since this signal is solely due to differences in surface albedo, we can deduce that clouds over polynyas are responsible for reducing the difference in the net shortwave budget by 69 W m^{-2} (or 40%).

Surprisingly, there is hardly a discernible impact of polynyas on the net longwave radiative budget at the surface (FLNS). FLNS is only slightly higher (6 EJ) during polynya years than during nonpolynya years; a difference that is reduced to 3 EJ at the top of the atmosphere (not shown).

A more detailed look at the components of the surface longwave balance (Fig. 4) shows that a rapid drop in upwelling longwave radiation (FLUS; Fig. 4b) during nonpolynya years is accompanied by an equally strong drop in downwelling longwave radiation (FLDS; Fig. 4c); the September values are 68 W m^{-2} lower for nonpolynya years than for polynya years. To understand
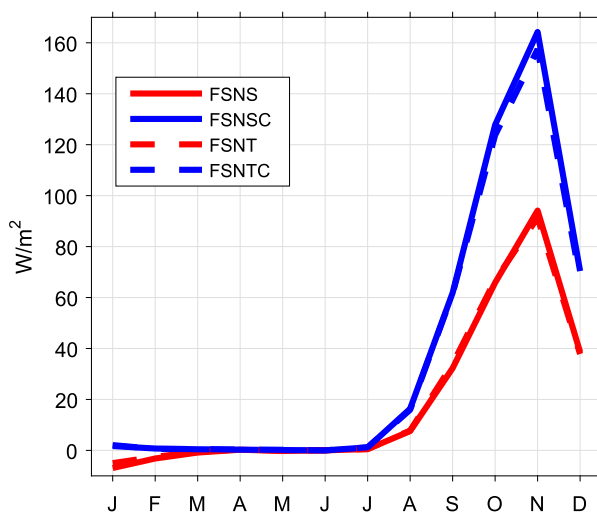

FIG. 3. Seasonal evolution of the difference in net shortwave balance between polynya and nonpolynya years. Shown are net shortwave at the surface under full-sky (FSNS) and clear-sky (FSNSC) conditions, and the same at the top of the atmosphere (FSNT, FSNTC).

the role of clouds in this response, we first consider the overall cloud fraction (CLDTOT). Figure 2 shows that cloud fraction is extremely high over the Antarctic ice pack in both polynya and nonpolynya years, with averages exceeding 97% in August. So the strong reduction in FLDS over sea ice cannot be explained by a reduction in the cloud fraction.

We analyze this issue further by considering the clear-sky fluxes. Figure 4c shows that the 68 W m^{-2} difference in downwelling longwave radiation in September (FLDS; solid lines) is reduced to only 30 W m^{-2} under clear-sky conditions (FLDSC; dashed lines); this difference must be attributed to the warmer atmosphere over polynyas. Differences in the cloud deck must hence be held responsible for the remaining 38 W m^{-2}. Indeed, the calculations show a systematic ~60 W m^{-2} drop in downwelling longwave flux over open water (red lines, Figs. 4c and 4d) when clouds are ignored; yet over sea ice, as typified by the winter–spring season during nonpolynya years, this difference is reduced to only 23 W m^{-2}. This shows that, in this model, the clouds over sea ice emit much less longwave radiation than the clouds over polynyas; despite the fact that both polynya and nonpolynya years feature almost permanent and complete cloud cover.

b. Vertical structure

Figure 4 shows that the largest seasonal changes in the longwave radiative fluxes are found during nonpolynya years, when the surface of the ocean transitions between ice-free and ice-covered states. It also suggests that this
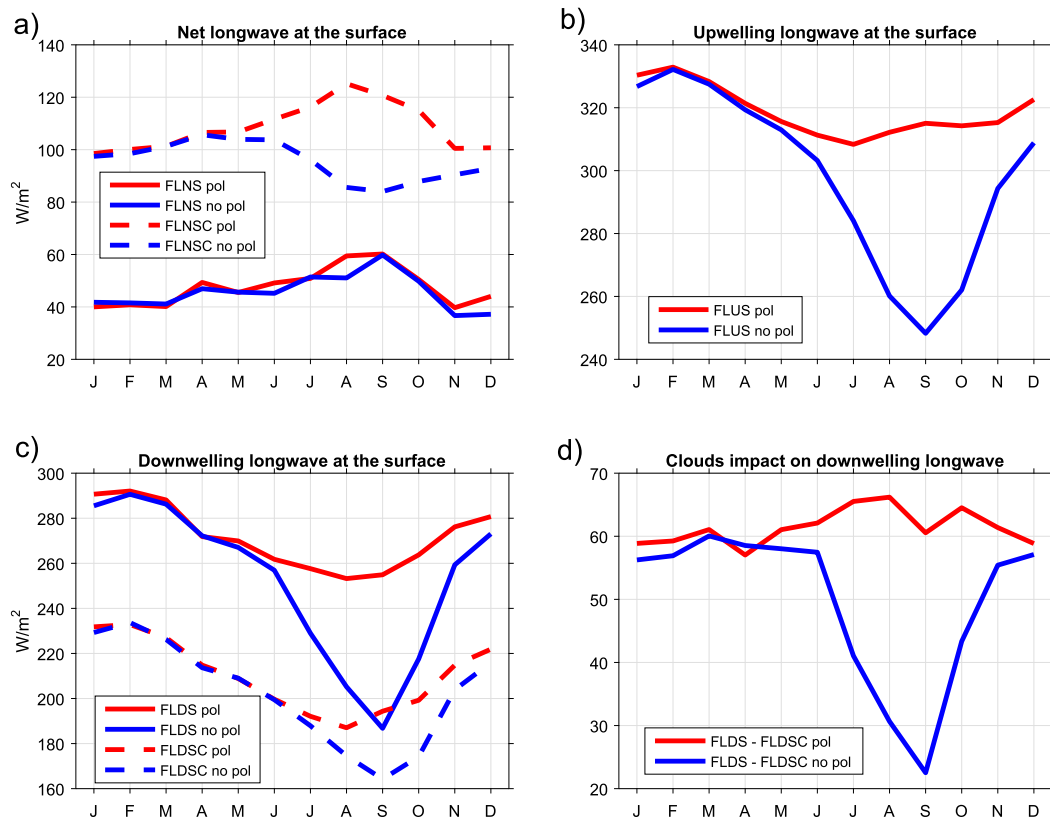
FIG. 4. Seasonal evolution of the different terms in the longwave radiative balance at the surface, averaged over the three polynya (red) and nonpolynya (blue) years. (a) Net longwave balance at the surface (FLNS) and the potential balance under clear-sky conditions (FLNSC); (b) outgoing longwave radiation (FLUS), calculated using the Stefan–Boltzmann law with emissivity of 1 (as used in the model for both open ocean and sea ice); (c) downwelling longwave at the surface (FLDS) and its clear-sky equivalent (FLDSC); and (d) the difference between FLDS and FLDSC, showing the impact of clouds on the downwelling longwave radiation.

is mainly caused by changes in the character of the cloud deck. In this section we look in more detail at the vertical structure of the atmosphere.

Figure 5 shows that there are significant differences in the vertical structure of the cloud deck between polynya and nonpolynya years. Cloud fraction (CLOUD) between 200 and 800 hPa hovers around 30% for nonpolynya years and is about 5% higher in polynya years. However, the largest difference is found below 800 hPa: polynya years have a maximum cloud fraction (68%) at 900 hPa, associated with a maximum in updraft (represented here by its associated heat transport −OMEGAT) and relative humidity (RELHUM). During nonpolynya years, on the other hand, maximum cloud fraction (60%) is found just above the surface, associated with a surface maximum in relative humidity and strongly reduced updraft. This is consistent with much more stable atmospheric conditions during nonpolynya years, as evidenced by the strongly reduced levels of turbulent kinetic energy (TKE).

There is also a significant difference in the cloud *composition*. In particular, the clouds during polynya years contain large amounts of water (ICLDLWP) and ice (ICLDIWP), in sharp contrast to the dry cloud deck during nonpolynya years. We deduce that the low water and ice content of the thinner cloud deck over sea ice is less able to absorb (re-emit) longwave radiation from (to) the surface than the optically thick cloud deck over open water. This allows the surface to cool more over sea ice, contributing to the reduction of the upwelling longwave radiation at the surface (FLUS in Fig. 4b). The resulting net longwave radiation at the surface (FLNS) is indistinguishable from that during polynya years (Fig. 4a).

c. Directional analysis

Figure 2 shows that there is no discernible impact of polynyas on SLP when considering monthly time scales. In this section we will look at this issue in more detail by analyzing how the atmospheric response to polynyas
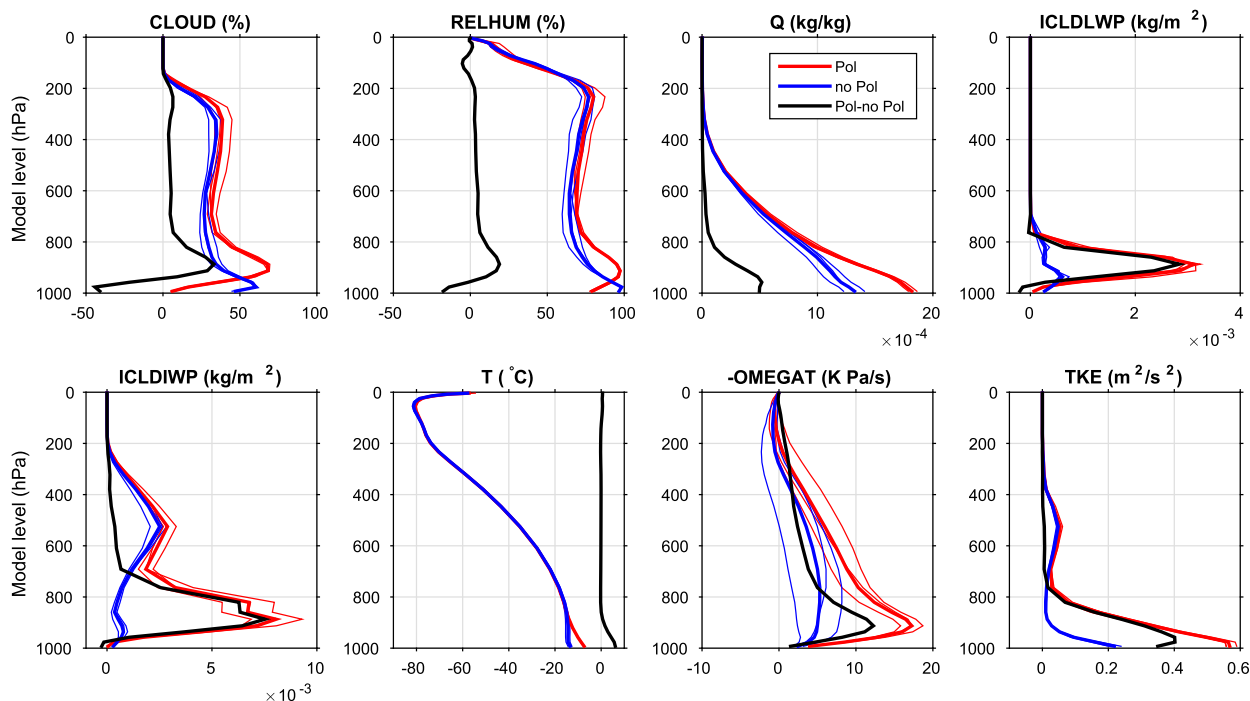
FIG. 5. Vertical profiles of ASO-averaged quantities, horizontally averaged over the polynya areas, for the three polynya years (thin red), the three nonpolynya years (thin blue), their averages (thick lines), and their difference (black). Variables shown are cloud fraction (CLOUD), relative humidity (RELHUM), specific humidity (Q), in-cloud liquid (ICLDLWP) and ice (ICLDIWP) water path, temperature (T), vertical heat advection ($-$OMEGAT), and turbulent kinetic energy (TKE).

depends on the wind direction on a daily time scale. To that end we categorize the available daily averaged fields according to prevailing wind direction over the polynya area, average over those directional subsets, and determine differences between polynya and non-polynya years (Fig. 6). Table 1 shows the number of days for each category for all polynya and nonpolynya years. The most prevalent wind conditions are southwesterly (SW) and quiet conditions (CE).

The table shows close tallies between polynya and nonpolynya years, so there is no indication that the presence of a polynya significantly affects the prevailing wind direction in the region. We can hence assume that the daily winds reflect synoptic atmospheric variability only. Interannual and large-scale variability in the atmosphere (like the SAM) could certainly exert a control on the presence of polynyas, and hence manifest itself in the difference between polynya and nonpolynya composites; but if such a control exists in this model, we would expect its expression to be indiscriminately present for all wind directions, and not be localized in the polynya region.

Note that only a few variables were saved on a daily basis, so this analysis is limited by data availability. Also, to focus on the regional response of SLP, we average daily SLP over our analysis region and remove this average from the daily SLP fields. This will remove the

impact of any large-scale or long-term influences, for instance climate drift.

For days with weak net winds (CE), the polynya is usually sandwiched between the westerlies to the north and easterlies to the south. The response patterns are mostly localized and limited to the polynya region, consistent with the large temperature difference over the polynya between the surface (mostly open water close to the freezing point) and the overlying atmosphere (TS $-$ TBOT). Sensible and latent heat fluxes (S + LHFLX), as well as 10-m wind speed (U10), are significantly enhanced when a polynya is present. We can also see a small but significant increase in precipitation, while there is no noticeable impact on SLP and hence on the large-scale circulation.

For northeasterly winds ($>$5 m s^{-1}; NE), the situation is more complex. These days are often associated with the arrival of a low pressure system from the west. Again, a large temperature difference and enhanced wind speeds lead to locally enhanced fluxes of sensible and latent heat (S + LHFLX). We also observe a large signature in near-surface humidity and precipitation, in particular in the region downwind from the polynya. In addition, there is a significant large-scale anomaly in sea level pressure, with elevated high pressure northwest of the polynya, and anomalously low pressure west of it.
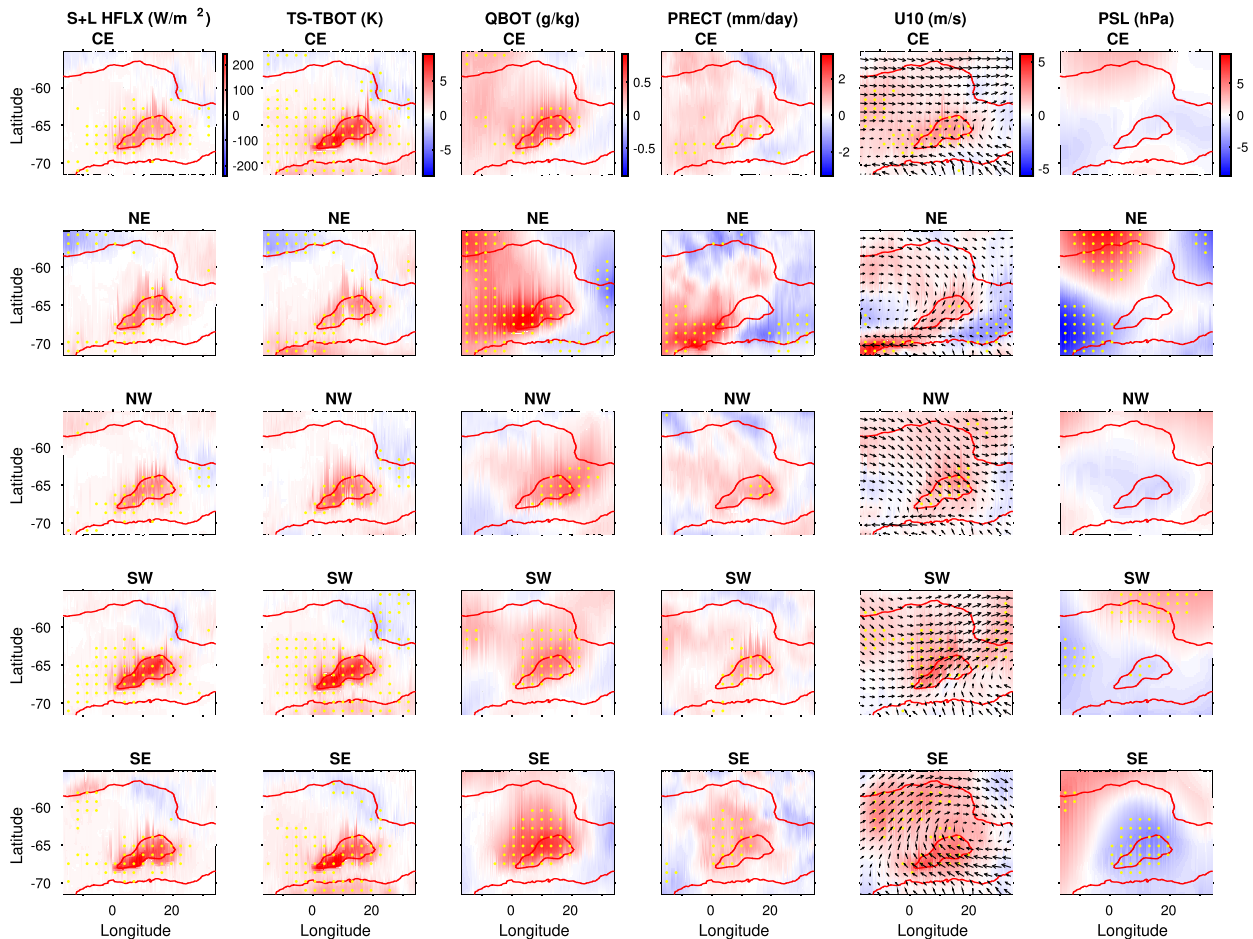
FIG. 6. Differences of atmospheric variables between polynya and nonpolynya years, separated according to daily wind direction. CE indicate averages over days with polynya-averaged wind speed smaller than $5\,\mathrm{m\,s^{-1}}$, regardless of direction. Other categories indicate averages over days with wind speeds exceeding $5\,\mathrm{m\,s^{-1}}$ and coming from the direction indicated. Yellow stippling indicates regions where the polynya and nonpolynya means are significantly different at 95%, according to a t test. Arrows in the "U10" plot indicate wind pattern averaged over the polynya years. Red contour indicates 45% contour of sea ice fraction averaged over polynya years (ASO only). Variables shown are the sum of sensible and latent heat fluxes (S + LHFLX), temperature difference between surface and atmosphere (TS − TBOT), humidity in the near-surface layer (QBOT), precipitation (PRECT), wind speed at 10 m (U10), and sea level pressure (PSL).

An illustrative synoptic case is shown in Fig. 7, which shows the evolution of the variables leading up to and following 19 September of polynya year 76, a day with northeasterly winds over the polynya. The day 18 September shows relatively quiet (CE) conditions over the polynya, with low wind speeds (U10), large air-sea temperature contrast (TS − TBOT), and large sensible and latent heat fluxes (S + LHFLX). The polynya is in the dry and cold continental air regime (low QBOT). On 19 September, a low pressure system arrives from the west, covering the polynya in moist and relatively warm maritime air (high QBOT). Despite the reduced air–sea temperature contrast, turbulent heat fluxes are still strong due to the higher wind speeds associated with the front. The depression accelerates the easterlies between the polynya and the continent (vectors in PSL panel)

and draws cold and dry continental air northward, resulting in relatively large ice–air temperature contrasts in the continental air zone just north of the continent. This air collides with the northeasterly flow of warm and moist maritime air, which gained moisture over the polynya. We surmise that this maritime air is forced upward, resulting in the band of strong precipitation southwest of the polynya. The following day, the depression has moved eastward, and so has the intensification of the easterlies. Precipitation has all but ceased. Although northeasterly wind events occur in both polynya and nonpolynya years, the atmospheric modification taking place over the polynyas apparently has a significant impact on the precipitation, intensification of the easterlies, and deepening of the atmospheric surface pressure just west of the polynya.

TABLE 1. Total number of days (percentage in brackets) for each wind direction category, for the ASO trimester of the three (left) polynya and (right) nonpolynya years. The total number of days in each column adds up to 276.

	No. of days in polynya years	No. of days in nonpolynya years
CE	75 (27%)	78 (28%)
NE	37 (13%)	36 (13%)
NW	53 (19%)	41 (15%)
SW	76 (28%)	82 (30%)
SE	35 (13%)	39 (14%)

For the northwesterly (NW), southwesterly (SW), and southeasterly (SE) wind directions (Fig. 6), the localized anomalies in sensible and latent heat fluxes, associated with the enhanced surface–air temperature contrast over polynyas, are clearly discernible. However, they are strongest for the southerly wind directions, when cold and dry continental air is advected northward over the polynya. We also see significantly enhanced humidity (QBOT) over the polynya, and in downstream plumes over the adjoining ice pack; enhanced wind speeds (U10); and enhanced precipitation, mostly on the downwind side of the polynya. For these three wind directions, surface pressure (SLP) shows a distinct minimum over the polynya. The difference in SLP between polynya and nonpolynya years is not significant for NW, slightly significant for SW, and quite pronounced for SE. This suggests that polynyas indeed exert an impact on the overlying atmosphere and the regional circulation.

4. Summary, discussion, and conclusions

In this article we analyzed output from a comprehensive synoptic-scale-resolving CESM simulation (Small et al. 2014) to study the response of the atmosphere to polynyas in the ice pack of the Lazarev Sea (between 0° and 14°E). We analyzed three years that featured a distinct and persistent polynya, and compared them to three years without a polynya. Although the relatively small sample size makes it difficult to make conclusive statements, several features emerged robustly from the analysis of this specific simulation:

- Sensible and latent heat fluxes are significantly enhanced over the polynya: peak monthly mean values are found in August, when sensible and latent heat fluxes reach 125 and 84 $W\,m^{-2}$, respectively (Bowen ratio $B = 1.5$); or 110 and 72 $W\,m^{-2}$ higher than during nonpolynya years. On a daily basis, these values are sensitive to the wind direction, as sensible and latent heat fluxes peak at 159 and 86 $W\,m^{-2}$, respectively, for southerly wind directions. These values are in good agreement with estimates by Moore et al. (2002), who studied the atmospheric response of the Weddell Polynya in an atmospheric reanalysis for the year 1976. They found sensible and latent heat fluxes of the order of 130 and 62 $W\,m^{-2}$, respectively ($B = 2.1$). In their analysis the peak fluxes occurred in June, whereas the model features the strongest fluxes in August.

- The polynya has a significant impact on the structure of the clouds, as the polynya is associated with a higher deck of convective clouds with high water and ice
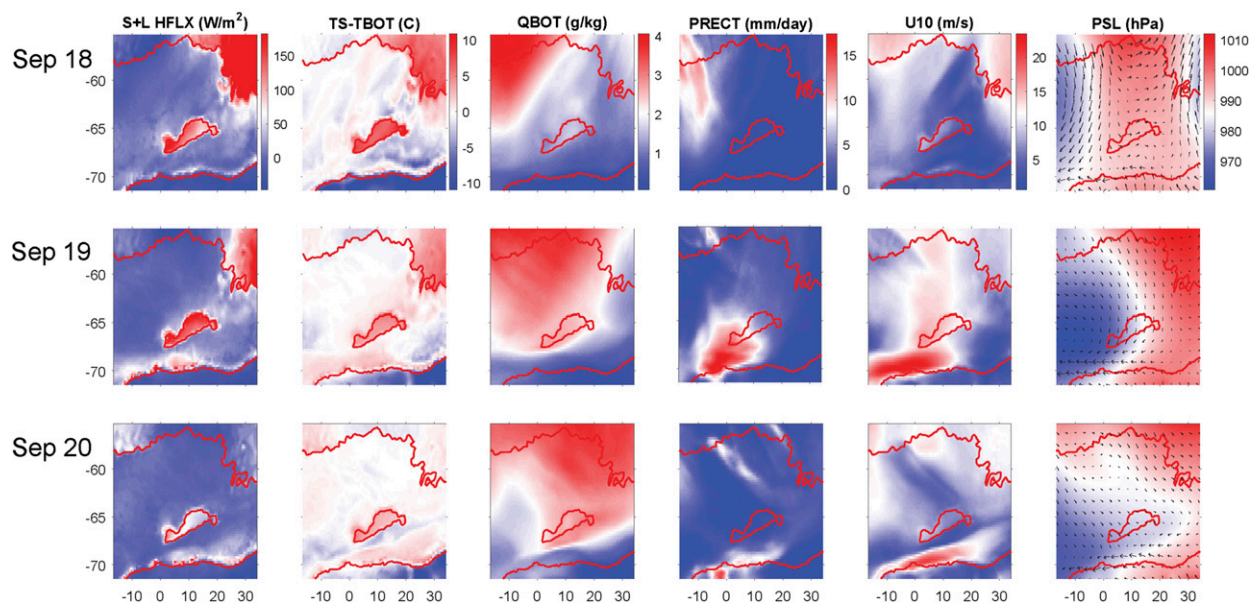

FIG. 7. Evolution of select variables for 18–20 Sep of polynya year 76.

content. Clouds in nonpolynya years, on the other hand, are lower to the ground and optically much thinner, and possibly reflect persistent ice fog (Girard and Blanchet 2001). In contrast to Moore et al. (2002), we did not find a significant difference in total cloud cover.

- Shortwave flux absorption is significantly enhanced over polynyas with a peak anomaly of about $94 \, \mathrm{W \, m^{-2}}$ in November, in agreement with Moore et al. (2002). This is due to the fact that the polynya's open water absorbs more solar radiation than sea ice, which has typical albedos varying between 0.3 and 0.5 for first-year ice, and up to 0.9 for snow covered ice (Brandt et al. 2005). Clear-sky calculations suggest that this difference could have been $164 \, \mathrm{W \, m^{-2}}$, but that the thicker cloud deck over polynyas prevents a significant fraction of the incoming solar radiation from reaching the surface.

- A remarkable finding of this study is that differences in the contributions to the surface longwave radiation budget seem to cancel out in this model. A sharp drop in outgoing longwave radiation during nonpolynya years is balanced by an equally strong decline in the downward longwave flux. We show that this decline results partly from a colder atmosphere that lacks the strong turbulent fluxes that warm up the atmosphere under polynya conditions, and partly from the optically much thinner clouds over sea ice that absorb much less of the (already reduced) upward longwave radiation. The net longwave balance shown by Moore et al. (2002) strongly resembles the net balance under clear-sky conditions in our model (dashed curves in Fig. 4a), with $40 \, \mathrm{W \, m^{-2}}$ stronger longwave emissions under polynya conditions.

- Specific humidity is significantly enhanced over the polynya and in downstream moisture plumes over the ice pack. Precipitation is also enhanced by about $1 \, \mathrm{mm \, day^{-1}}$, in agreement with Moore et al. (2002). This enhancement takes place mostly on the downwind side, where we indeed expect uplift (Dare and Atkinson 1999).

- We found some support for the hypothesis that the polynya generates a thermal low pressure system, as predicted by Timmermann et al. (1999). However, this response was found to be statistically significant only for southerly wind directions that advect cold and dry continental air over the polynya. Moore et al. (2002) find 6–8-mbar lower sea level pressure over the Weddell Polynya compared to climatology, while Glowienka-Hense (1995) find values between 3 and 4 mbar; our values for southerly winds are more in line with the latter.

We found that the simulated winter cloud cover in the model is very high (up to 95%) for both polynya and nonpolynya years. This is at odds with the reanalysis results from Moore et al. (2002) who show cloud fractions between 60% and 70% for the 1976 Weddell Polynya, and around 40% for the nonpolynya climatology. The high cloud fractions during polynya years may be rather realistic. Although remote sensing of clouds was in its infancy in the mid-1970s, Carsey (1980, p. 2034) notes that the cloudiness over the Weddell Polynya was very high ("100% on most days"). Bromwich et al. (2012) compares more recent satellite observations for the post-Weddell Polynya era and finds high (>90%) cloud fractions just north of the sea ice zone, which may be a reasonable proxy for polynya conditions. The modeled cloud fractions during the nonpolynya situations, on the other hand, appear to be higher than observations suggest. Bromwich et al. (2012) find cloud fractions generally between 70% and 85% for the September–October–November trimester in the general area of our modeled polynya in the Lazarev Sea. This is in agreement with Guest (1998), who observed overcast conditions 77% of the time over the ice pack in July–August 1994. So either the modeled fraction of the clouds during non-polynya situations (>90%) is unrealistically high, or their low optical thickness makes them hard to detect using satellite remote sensing. In terms of their vertical distribution the model seems to agree with observations from the Cloud-Aerosol lidar and Infrared Pathfinder Satellite Observation (CALIPSO) satellite that show that low clouds contribute most, up to 70% (Chepfer et al. 2010).

A few studies present measurements of longwave radiative balance in the Southern Ocean. Yamanouchi and Charlock (1997) present longwave radiative fluxes at the top of the atmosphere from the Earth Radiation Budget Experiment (ERBE). Their data from the region of our polynya shows a good match to the longwave fluxes at the top of the model (FLNT; not shown); in particular a seasonal cycle that varies between 180 and $220 \, \mathrm{W \, m^{-2}}$ with a minimum in July–August. Guest (1998) discusses in situ observations from within the ice pack of the Maud Rise region during the Antarctic Zone Flux Experiment (ANZFLUX) in July and August of 1994. He observed overcast skies 77% of the time, and clear skies 10% of the time, and found a $62 \, \mathrm{W \, m^{-2}}$ difference in downwelling longwave radiation between those conditions. This number agrees with the $60–65 \, \mathrm{W \, m^{-2}}$ cloud radiative forcing (Fig. 4d) for polynya situations in our model, but is higher than the $23 \, \mathrm{W \, m^{-2}}$ for nonpolynya years. Under clear-sky conditions he observes a net longwave budget of $87 \, \mathrm{W \, m^{-2}}$, which agrees well with the $\sim 90 \, \mathrm{W \, m^{-2}}$ clear-sky values for July and August in our model (blue dashed in Fig. 4a). This suggests that the cloud deck observed by Guest (1998) is optically much thicker than the clouds simulated in our model for nonpolynya situations.

Although Guest (1998) does not mention an *average* net longwave balance for his month-long time series, we

can crudely estimate one from his histogram of net longwave radiation occurrences. If 77% prevalence of overcast skies represents a $20 \, \mathrm{W \, m^{-2}}$ net longwave balance on average, 10% occurrence of clear skies about $90 \, \mathrm{W \, m^{-2}}$, and the remaining 13% about $50 \, \mathrm{W \, m^{-2}}$, we can infer an average net balance of about $31 \, \mathrm{W \, m^{-2}}$. This is approximately a factor of 2 lower than either polynya or nonpolynya conditions in our model ($\sim$50–60 $\mathrm{W \, m^{-2}}$ in July and August), and would represent a 10% bias in downwelling longwave radiation.

We found that the northeasterly wind direction generates the strongest response of the atmosphere, with a significant strengthening of the easterlies adjacent to the continent, and a downstream plume of precipitation that is apparently generated by the uplift of the warm and moisture-laden polynya air when it collides with the continental winds. The response of the atmospheric pressure pattern shows a significant lowering of the PSL downstream of the polynya. This pattern is robustly reproduced, even after subsampling the NE days every third day. The dynamics of this response is not clear and will require further analysis and experimentation.

This study confirms that large open-ocean polynyas have a significant local impact on the overlying atmosphere. Regional-scale impacts are also clear from the current analysis, but depend strongly on the synoptic wind direction. Most notably this study reveals the usefulness of analyzing the output of state-of-the-art high-resolution earth system models (ESMs) to enhance our understanding of intricate coupled phenomena that may simply not emerge in coarse-resolution ESM simulations. Here, we first find that a polynya emerges only in the high-resolution simulations, which in its own right is an issue to be investigated. Second, the high spatial resolution of the atmosphere component (CAM5) allows for detailed investigations of the polynya impact on the atmosphere in a coupled setting.

REFERENCES

Adolphs, U., and G. Wendler, 1995: A pilot study on the interactions between katabatic winds and polynyas at the Adélie Coast, eastern Antarctica. *Antarct. Sci.*, **7**, 307–314, doi:10.1017/S0954102095000423.

Andreas, E. L, W. B. Tucker, and S. F. Ackley, 1984: Atmospheric boundary-layer modification, drag coefficient, and surface heat flux in the Antarctic marginal ice zone. *J. Geophys. Res.*, **89**, 649–661, doi:10.1029/JC089iC01p00649.

Arbetter, T. E., A. H. Lynch, and D. A. Bailey, 2004: Relationship between synoptic forcing and polynya formation in the Cosmonaut Sea: 1. Polynya climatology. *J. Geophys. Res.*, **109**, C04022, doi:10.1029/2003JC001837.

Arrigo, K. R., and G. L. Van Dijken, 2003: Phytoplankton dynamics within 37 Antarctic coastal polynya systems. *J. Geophys. Res.*, **108**, 3271, doi:10.1029/2002JC001739.

Bailey, D. A., A. H. Lynch, and T. E. Arbetter, 2004: Relationship between synoptic forcing and polynya formation in the Cosmonaut Sea: 2. Regional climate model simulations. *J. Geophys. Res.*, **109**, C04023, doi:10.1029/2003JC001838.

Brandt, R. E., S. G. Warren, A. P. Worby, and T. C. Grenfell, 2005: Surface albedo of the Antarctic sea ice zone. *J. Climate*, **18**, 3606–3622, doi:10.1175/JCLI3489.1.

Bromwich, D. H., and Coauthors, 2012: Tropospheric clouds in Antarctica. *Rev. Geophys.*, **50**, RG1004, doi:10.1029/2011RG000363.

Carsey, F., 1980: Microwave observation of the Weddell Polynya. *Mon. Wea. Rev.*, **108**, 2032–2044, doi:10.1175/1520-0493(1980)108<2032:MOOTWP>2.0.CO;2.

Cheon, W. G., Y.-G. Park, J. Toggweiler, and S.-K. Lee, 2014: The relationship of Weddell Polynya and open-ocean deep convection to the Southern Hemisphere westerlies. *J. Phys. Oceanogr.*, **44**, 694–713, doi:10.1175/JPO-D-13-0112.1.

——, S.-K. Lee, A. L. Gordon, Y. Liu, C.-B. Cho, and J. J. Park, 2015: Replicating the 1970's Weddell Polynya using a coupled ocean-sea ice model with reanalysis surface flux fields. *Geophys. Res. Lett.*, **42**, 5411–5418, doi:10.1002/2015GL064364.

Chepfer, H., S. Bony, D. Winker, G. Cesana, J. Dufresne, P. Minnis, C. Stubenrauch, and S. Zeng, 2010: The GCM-Oriented CALIPSO Cloud Product (CALIPSO-GOCCP). *J. Geophys. Res.*, **115**, D00H16, doi:10.1029/2009JD012251.

Comiso, J. C., and A. L. Gordon, 1987: Recurring polynyas over the Cosmonaut Sea and the Maud Rise. *J. Geophys. Res.*, **92**, 2819–2834, doi:10.1029/JC092iC03p02819.

——, and ——, 1996: Cosmonaut polynya in the Southern Ocean: Structure and variability. *J. Geophys. Res.*, **101**, 18 297–18 313, doi:10.1029/96JC01500.

Dare, R., and B. Atkinson, 1999: Numerical modeling of atmospheric response to polynyas in the Southern Ocean sea ice zone. *J. Geophys. Res.*, **104**, 16 691–16 708, doi:10.1029/1999JD900137.

——, and ——, 2000: Atmospheric response to spatial variations in concentration and size of polynyas in the Southern Ocean sea-ice zone. *Bound.-Layer Meteor.*, **94**, 65–88, doi:10.1023/A:1002442212593.

de Lavergne, C., J. B. Palter, E. D. Galbraith, R. Bernardello, and I. Marinov, 2014: Cessation of deep convection in the open Southern Ocean under anthropogenic climate change. *Nat. Climate Change*, **4**, 278–282, doi:10.1038/nclimate2132.

Delworth, T. L., and Coauthors, 2012: Simulated climate and climate change in the GFDL CM2.5 high-resolution coupled climate model. *J. Climate*, **25**, 2755–2781, doi:10.1175/JCLI-D-11-00316.1.

Downes, S. M., and Coauthors, 2015: An assessment of Southern Ocean water masses and sea ice during 1988–2007 in a suite of

interannual CORE-II simulations. *Ocean Modell.*, **94**, 67–94, doi:10.1016/j.ocemod.2015.07.022.

Girard, E., and J.-P. Blanchet, 2001: Microphysical parameterization of Arctic diamond dust, ice fog, and thin stratus for climate models. *J. Atmos. Sci.*, **58**, 1181–1198, doi:10.1175/1520-0469(2001)058<1181:MPOADD>2.0.CO;2.

Glowienka-Hense, R., 1995: GCM response to an Antarctic polynya. *Contrib. Atmos. Phys.*, **68**, 303–317.

Gordon, A. L., 1982: Weddell deep water variability. *J. Mar. Res.*, **40**, 199–217.

——, 2014: Oceanography: Southern Ocean polynya. *Nat. Climate Change*, **4**, 249–250, doi:10.1038/nclimate2179.

——, and W. F. Haxby, 1990: Agulhas eddies invade the South Atlantic: Evidence from GEOSAT altimeter and shipboard CTD survey. *J. Geophys. Res.*, **95**, 3117–3125, doi:10.1029/JC095iC03p03117.

——, M. Visbeck, and J. C. Comiso, 2007: A possible link between the Weddell Polynya and the southern annular mode. *J. Climate*, **20**, 2558–2571, doi:10.1175/JCLI4046.1.

Griffies, S. M., and Coauthors, 2015: Impacts on ocean heat from transient mesoscale eddies in a hierarchy of climate models. *J. Climate*, **28**, 952–977, doi:10.1175/JCLI-D-14-00353.1.

Guest, P. S., 1998: Surface longwave radiation conditions in the eastern Weddell Sea during winter. *J. Geophys. Res.*, **103**, 30 761–30 771, doi:10.1029/98JC02146.

Heuzé, C., K. J. Heywood, D. P. Stevens, and J. K. Ridley, 2013: Southern Ocean bottom water characteristics in CMIP5 models. *Geophys. Res. Lett.*, **40**, 1409–1414, doi:10.1002/grl.50287.

Holland, D. M., 2000: Transient sea-ice polynya forced by oceanic flow variability. *Prog. Oceanogr.*, **48**, 403–460, doi:10.1016/S0079-6611(01)00010-6.

——, 2001: Explaining the Weddell Polynya—A large ocean eddy shed at Maud Rise. *Science*, **292**, 1697–1700, doi:10.1126/science.1059322.

Hurrell, J. W., and Coauthors, 2013: The Community Earth System Model: A framework for collaborative research. *Bull. Amer. Meteor. Soc.*, **94**, 1339–1360, doi:10.1175/BAMS-D-12-00121.1.

Johnson, G. C., 2008: Quantifying Antarctic Bottom Water and North Atlantic Deep Water volumes. *J. Geophys. Res.*, **113**, C05027, doi:10.1029/2007JC004477.

Kay, J., and Coauthors, 2012: Exposing global cloud biases in the Community Atmosphere Model (CAM) using satellite observations and their corresponding instrument simulators. *J. Climate*, **25**, 5190–5207, doi:10.1175/JCLI-D-11-00469.1.

——, and Coauthors, 2015: The Community Earth System Model (CESM) large ensemble project: A community resource for studying climate change in the presence of internal climate variability. *Bull. Amer. Meteor. Soc.*, **96**, 1333–1349, doi:10.1175/BAMS-D-13-00255.1.

——, C. Wall, V. Yettella, B. Medeiros, C. Hannay, P. Caldwell, and C. Bitz, 2016: Global climate impacts of fixing the Southern Ocean shortwave radiation bias in the Community Earth System Model (CESM). *J. Climate*, **29**, 4617–4636, doi:10.1175/JCLI-D-15-0358.1.

Kirtman, B. P., and Coauthors, 2012: Impact of ocean model resolution on CCSM climate simulations. *Climate Dyn.*, **39**, 1303–1328, doi:10.1007/s00382-012-1500-3.

Komurcu, M., and Coauthors, 2014: Intercomparison of the cloud water phase among global climate models. *J. Geophys. Res. Atmos.*, **119**, 3372–3400, doi:10.1002/2013JD021119.

Maqueda, M., A. Willmott, and N. Biggs, 2004: Polynya dynamics: A review of observations and modeling. *Rev. Geophys.*, **42**, RG1004, doi:10.1029/2002RG000116.

Martinson, D. G., P. D. Killworth, and A. L. Gordon, 1981: A convective model for the Weddell Polynya. *J. Phys. Oceanogr.*, **11**, 466–488, doi:10.1175/1520-0485(1981)011<0466:ACMFTW>2.0.CO;2.

McClean, J. L., and Coauthors, 2011: A prototype two-decade fully-coupled fine-resolution CCSM simulation. *Ocean Modell.*, **39**, 10–30, doi:10.1016/j.ocemod.2011.02.011.

Moore, G., K. Alverson, and I. Renfrew, 2002: A reconstruction of the air–sea interaction associated with the Weddell Polynya. *J. Phys. Oceanogr.*, **32**, 1685–1698, doi:10.1175/1520-0485(2002)032<1685:AROTAS>2.0.CO;2.

Prasad, T., J. L. McClean, E. C. Hunke, A. J. Semtner, and D. Ivanova, 2005: A numerical study of the western Cosmonaut polynya in a coupled ocean–sea ice model. *J. Geophys. Res.*, **110**, C10008, doi:10.1029/2004JC002858.

Small, R. J., and Coauthors, 2014: A new synoptic scale resolving global climate simulation using the Community Earth System Model. *J. Adv. Model. Earth Syst.*, **6**, 1065–1094, doi:10.1002/2014MS000363.

Smith, S. D., R. D. Muench, and C. H. Pease, 1990: Polynyas and leads: An overview of physical processes and environment. *J. Geophys. Res.*, **95**, 9461–9479, doi:10.1029/JC095iC06p09461.

Smith, W. O., Jr., and L. I. Gordon, 1997: Hyperproductivity of the Ross Sea (Antarctica) polynya during austral spring. *Geophys. Res. Lett.*, **24**, 233–236, doi:10.1029/96GL03926.

Stössel, A., K. Yang, and S.-J. Kim, 2002: On the role of sea ice and convection in a global ocean model. *J. Phys. Oceanogr.*, **32**, 1194–1208, doi:10.1175/1520-0485(2002)032<1194:OTROSI>2.0.CO;2.

——, D. Notz, F. A. Haumann, H. Haak, J. Jungclaus, and U. Mikolajewicz, 2015: Controlling high-latitude Southern Ocean convection in climate models. *Ocean Modell.*, **86**, 58–75, doi:10.1016/j.ocemod.2014.11.008.

Tan, I., T. Storelvmo, and M. D. Zelinka, 2016: Observational constraints on mixed-phase clouds imply higher climate sensitivity. *Science*, **352**, 224–227, doi:10.1126/science.aad5300.

Timmermann, R., P. Lemke, and C. Kottmeier, 1999: Formation and maintenance of a polynya in the Weddell Sea. *J. Phys. Oceanogr.*, **29**, 1251–1264, doi:10.1175/1520-0485(1999)029<1251:FAMOAP>2.0.CO;2.

von Storch, H., and F. W. Zwiers, 1999: *Statistical Analysis in Climate Research*. Cambridge University Press, 484 pp.

Williams, W., E. Carmack, and R. Ingram, 2007: Physical oceanography of polynyas. *Polynyas: Windows to the World*, W. O. Smith and D. G. Barber, Eds., Elsevier Oceanography Series, Vol. 74, Elsevier, 55–85, doi:10.1016/S0422-9894(06)74002-8.

Yamanouchi, T., and T. P. Charlock, 1997: Effects of clouds, ice sheet, and sea ice on the Earth radiation budget in the Antarctic. *J. Geophys. Res.*, **102**, 6953–6970, doi:10.1029/96JD02866.

Zwally, H. J., and P. Gloersen, 1977: Passive microwave images of the polar regions and research applications. *Polar Rec.*, **18**, 431–450, doi:10.1017/S0032247400000930.

——, J. Comiso, and A. Gordon, 1985: Antarctic offshore leads and polynyas and oceanographic effects. *Oceanology of the Antarctic Continental Shelf*, S. S. Jacobs, Ed., Amer. Geophys. Union, 203–226, doi:10.1029/AR043p0203.